Bioprinting 21 (2021) e00112

Contents lists available at ScienceDirect

Bioprinting

journal homepage: www.elsevier.com/locate/bprint

Image analysis as PAT-Tool for use in extrusion-based bioprinting

Svenja Strauß [a], Rafaela Meutelet [a], Luka Radosevic [a], Sarah Gretzinger [a,b], Jürgen Hubbuch [a,b,*]

[a] Karlsruhe Institute of Technology, Institute of Functional Interfaces, Karlsruhe, Germany
[b] Institute of Engineering in Life Sciences, Section IV: Molecular Separation Engineering, Karlsruhe Institute of Technology, Karlsruhe, Germany

ARTICLE INFO

Keywords:
Automated image processing
Line or extrusion characterization
Printing process development
Bioprinting

ABSTRACT

The technology of bioprinting is arousing a growing interest in biopharmaceutical research and industry. In order to accelerate process development in the field of bioprinting, image-based analysis methods are non-invasive, time- and cost-saving tools which are useable for printer characterization, bioink printability evaluation, and process optimization. Image processing can also be used for the study of reproducibility, since reliable production is important in the transition from research to industrial application, and more precisely to clinical studies. This study revolves around the establishment of an automated and image-based line analysis method for bioprinting applications which enables an easy comparison of 3D-printed lines. Diverse rheological properties of bioinks and the printing process affect the geometry of the resulting object. The line represents a simple geometry, where the influence of the rheological properties and printing parameters is directly apparent. Therefore, a method for line analysis was developed on the basis of image recognition. At first, the method is tested for several substances such as Nivea®, pure and colored Kolliphor solutions, and two commercially available hydrogel formulations which can be used as bioinks. These are Biogelx™-ink-RGD by Biogelx and Cellink® Bioink by Cellink. The examination of limitations showed that transparent materials such as Kolliphor-based solutions cannot be analyzed with the developed method whereas opaque materials such as Nivea® and both bioinks can be analyzed. In the course of process characterization, the method was used to investigate the shrinkage behavior for both bionks. With the help of the line analysis tool, a shrinkage behavior of both bioinks was demonstrated and thus, process time could be identified as a critical process parameter.

1. Introduction

In recent developments, bioprinting is arising in the field of regenerative medicine (RM) and tissue engineering (TE) [1,2]. The use of 3D-printing technology allows additive manufacturing (AM) of artificial tissues in a layer-by-layer deposition of materials containing cells [3]. These artificial tissues are promising for patient-specific implants which can be employed as tissue replacement or as drug delivery systems [4]. Furthermore, tissue models can be used for clinical and pharmaceutical studies as they are mimicking natural living conditions [5,6]. The lack of tissue-specific bioinks with suitable properties represents a major issue in development [7]. On the one hand, bioinks have to be optimized in terms of printability and shape accuracy. On the other hand, mild conditions must be guaranteed, as the bioink contains cells and biological material [8]. Due to their high water content, bioinks mainly consist of hydrogels which are water-containing but water-insoluble polymers whose molecules are crosslinked to form a three-dimensional network. The network can be designed for immobilzation of cells and biologic macromolecules, while enabling diffusion of substrates and products [9,10]. Therefore, it is important to know and control the width of a printed element to avoid mass transfer limitations in printed systems containing cells [11]. The used polymers can be either synthetic, such as polyethylene glycol (PEG), or of natural origin [12,13]. Natural polymers can be divided into polymers of polysaccharides (like alginate, chitosan, dextran, and hyaluronic acid) and protein-based polymers (like gelatine and collagen) [14–20]. It is assumed that natural polymers have a good biocompatibility and do not trigger an inflammatory reaction of the immune system [21]. Depending on the application, hydrogels are modified, e.g. by incorporation of ligands and copolymers. This allows a better control of the number and size of meshes, biodegradation, and cell adhesion [22–25]. The different origins and modifications result in diverse optical properties of the hydrogels from completely transparent like gelatine to opaque and white [26].

In addition, each specific tissue has different requirements, e.g.,

* Corresponding author. Institute of Engineering in Life Sciences, Section IV: Biomolecular Separation Engineering, Karlsruhe Institute of Technology (KIT), Fritz-Haber-Weg 2, 76131, Karlsruhe, Germany.
E-mail address: juergen.hubbuch@kit.edu (J. Hubbuch).

https://doi.org/10.1016/j.bprint.2020.e00112
Received 12 August 2020; Received in revised form 3 November 2020; Accepted 4 November 2020

mechanical integrity and stability, and a universal bioink is most likely not to be found [3]. A general problem is the absence of standardized analytical methods to simplify the comparability and selection of bioinks. For bioink characterization, rheological measurements have been established to determine the printability and behavior during extrusion [27–30]. However, the exact printing parameters cannot yet be derived from the rheological properties. Bioprintability is classified by checking the bioprinted object in comparison to the given computer-aided design (CAD) model [31,32]. Another rather qualitative approach is to use overhanging structures to test filament collapse and to compare the degree of strand fusion of parallel printed filaments [33]. These examinations are carried out offline and sometimes take a long time, so that no high-throughput analysis is possible. Image-based methods offer other options as they evaluate large data sets automatically. Online monitoring with a camera system is also conceivable. The analysis of images cannot only be used for classifying the printability of bioinks, but also for printer characterization and printing process optimization in a standardized way. Image processing is widely used for quality inspection in production processes in several industries such as the printing and packaging industry and the automotive industry, and also, medical image processing is used for diagnostic purposes [34,35]. In the field of 3D-printing, image analysis is already being investigated for characterization of the strands generated by melt electro writing [36]. The printability and shape accuracy of bioinks is often evaluated by analyzing the shape of an extruded strand and measuring the widths and angles of extruded objects after bioprinting [31,37–39]. The measurement takes place individually and manually by marking the widths in a software [40]. Consequently, these methods are susceptible to differences when used by different users. Even simple line width determination is prone to errors as the width can be influenced by the local measurement point at which it is measured because not all lines must have constant widths at every position. In the light of the above and even though we are standing on a new aera of bioprinting as a production and formulation tool in the fields of regenerative medicine (RM) and tissue engineering (TE) [1,2] process analytics are not present or ready for it. The aim of this study is to establish an automated image-based line analysis tool which measures line width, length, and area based on images of extruded bioink strands in a standardized way, where line width measurements are only possible within a defined stable area. The intention is to establish a method which can be used to recognize the impact of changes in bionk formulation, in printer systems, and on the outcome of printing processes. This PAT-tool was then used to measure the shrinkage behavior of bioinks to evaluate if the process time is a critical process parameter as bioinks might dehydrate over time.

2. Materials and methods

2.1. Bioprint substances and bioink preparation

Syringes including pistons were ordered from Nordson Corporation (Westlake, USA) and six-well glass bottom plates were purchased from IBL Baustoff + Labor GmbH (Gerasdorf, Austria). Conical 25 G nozzles were obtained from Cellink (Gothenburg, Sweden). As printed substances, Nivea® Creme by Beiersdorf AG (Hamburg, Germany) and a solution of 30% (w/w) Kolliphor P 407 (Sigma-Aldrich, USA) dissolved in ultrapure water (arium® pro VF, Satorius AG, Göttingen, Germany) were used. Two commercially available bioinks, namely Cellink® Bioink (Cellink, Gothenburg, Sweden) and Biogelx™-ink-RGD (Biogelx Ltd, Newhouse, United Kingdom) were also printed. According to manufacturer specification, 149 mg bioink powder were dissolved in 2.25 ml of the kit's solution B and were kept in the refrigerator over night at 4 °C. Then, the solution was mixed with 1.25 ml of Dulbecco's Modified Eagle's Medium (DMEM) (ThermoFisher Scientific, Waltham, USA) and incubated for 2h at 37 °C. 30% (w/w) Kolliphor solution as base and manufactured as described in the upper section was colored with different dyes to increase contrast. Therefore, a solution of 2.5% (w/w) red powder food coloring (Brauns Heitmann GmbH & Co. KG, Warburg, Germany), a solution of 2.5% (w/w) red paste-like food coloring (Dr. August Oetker Nahrungsmittel KG, Bielefeld, Germany), and a solution with a spike by Sicopharm Cochineal Red (BASF, Ludwigshafen, Germany) were produced.

2.2. Bioprinting process

All 3D-printing experiments were carried out with a pneumatic extrusion-based bioprinter 3D Discovery™ provided by regenHU company (Villaz-St-Pierre, Switzerland). With the BioCAD software (regenHU, Villaz-St-Pierre, Switzerland), 3 cm long lines were designed and printed in each welll of a six-well plate. The respective printing parameters of materials are listed in Table 1.

2.3. Image processing

Images of the printed lines were taken using the microplate reader Spark® provided by Tecan Group AG (Männedorf, Switzerland), and each well was measured using the cell confluence method in the SparkControl Software™ (Tecan Group AG, Männedorf, Switzerland). Two image files were generated as output files. One has already been analyzed by the software and one is comparable to a stitched microscope image in grayscale which was imported into Matlab® R2019a (TheMathWorks, Natick, USA) for further study. The image processing sequence is shown schematically in Fig. 1 a).

b) shows exemplarily the image processing: The original image is converted to binary, the image is segmented, and small objects are deleted. Then, a histogram is created by counting and converting pixels per column. Area and length can be determined. Line width is only determined if a plateau containing a stable area is found.

Before processing the images, the file directory is chosen, the reference width which is equal to the nozzle diameter and the conversion factor from pixel to millimeter are imported. The image processing is shown by an example image in Fig. 1 b). Initially, the original image is read in and converted into a binary image. Then, the image is segmented by deleting small objects, clearing the boarders and detecting the object. As the limitations of the method were also investigated and this is a critical step, a user query was here introduced. After the user's confirmation of correct line detection, the actual line analysis starts. At first, a histogram is created by counting white pixels for each column and by converting them in millimeters. The length is calculated as the number of white pixel columns and the area is determined as the conversion of the sum of all white pixels in all columns as described in Euqations 1 and 2.

$$length = number\ of\ columns\ containing\ white\ pixels \cdot conversion\ factor \quad (1)$$

$$area = \sum white\ pixels \cdot conversion\ factor^2 \quad (2)$$

In order to measure the width, the corner points in the first and last third of the histogram are recognized and the distance between the corner points is isolated as a plateau. This plateau will be further examined if there is a stable area which is useful for a line width

Table 1
Printing parameters of the respective materials. Pure and all colored Kolliphor-based solutions were printed with similar parameters.

Parameter	Nivea	Kolliphor hydrogels	Cellink Bioink	Biogelx-ink-RGD
Pressure [MPa]	0.33	0.13	0.03	0.025
Speed [mm/s]	30	10	10	10
Layer height [mm]	0.1	0.1	0.1	0.1
Offset [mm]	0.05	0.05	0.05	0.05

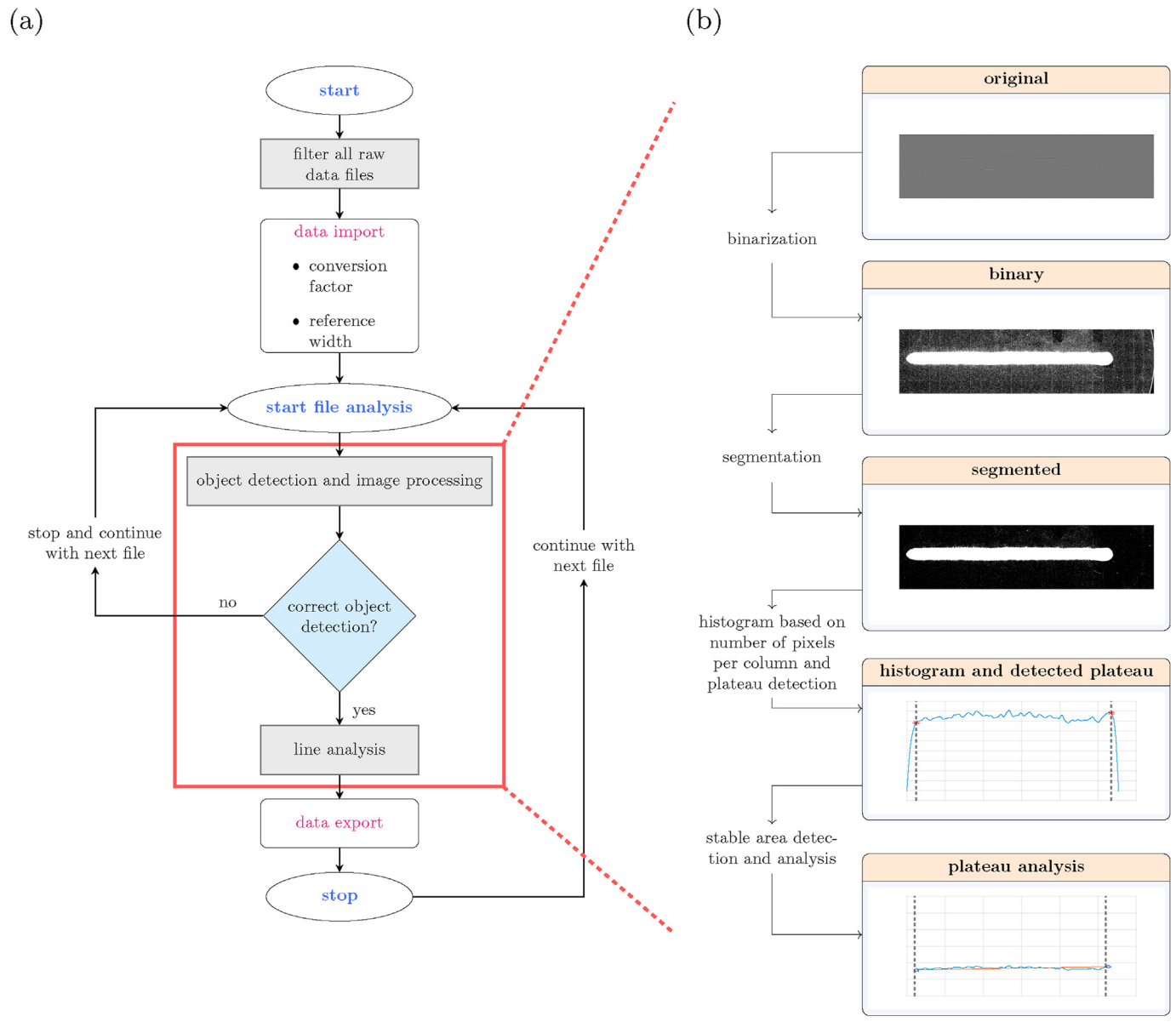

Fig. 1. Overview of the data and image processing: a) represents a schematic flow chart of data processing. At first, raw image files are filtered and application-specific parameters are imported. Each file is analyzed individually in a loop in which the user has to confirm or deny correct object detection. In the case of correct object detection the actual line analysis starts. At the end, all results are saved and exported for each file.

determination. The plateau is divided into 10 parts and for each section, the slope, which is ideally 0, is calculated individually. A tolerance criterion was introduced; it is shown in Equation (3).

$$tol = \frac{\frac{deviation}{l}}{reference\ width} \tag{3}$$

The tolerance (tol) is defined as the permitted percentage deviation of the reference width per the length of 1 mm strand (l). Consequently, the tolerance is dependent on the nozzle diameter and is higher with a bigger diameter. A deviation of 3% was used, and the reference width corresponds to the nozzle diameter of 0.26 mm. As long as the slope of the section was within this tolerance, the section extended constantly to both sides and the slope was calculated for each extension until the criterion was no longer met or the edge was reached. If the length was greater than 5 mm, it was determined as a stable area and the line width was calculated by averaging the values of the section. Otherwise, the line was not considered constant and a line width determination was not possible.

2.4. Shrinkage study

Three cartridges by Cellink® Bioink and Biogelx™-ink-RGD (n = 3) were prepared on three different days for investigating the drying and shrinkage behavior of bioinks. Each cartridge was used for printing in each well of one six-well plate (n = 6) so that in total 18 lines were printed for each bioink. A schematic representation is shown in Fig. 2.

The plates were analyzed after 0, 2, 5, and 10min as described in Section 2.3.

2.5. Data analysis and statistical analysis

Data evaluation, image processing, statistical data analysis, and visualization were done with Matlab® R2019a (TheMathWorks, Natick, USA). In the case of failed object detection, data were examined for outliers and these were removed if they deviated from the median by more than three scaled mean absolute deviations. All results for one property obtained from one plate were checked for normal distribution

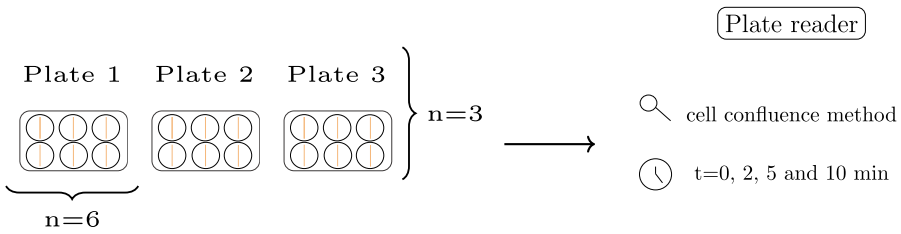

Fig. 2. Schematic process of the shrinkage study: 3 cartridges were prepared as biological replicate (n = 3) and with each cartridge one plate was printed containing 6 lines as technical replicate (n = 6) so that in total 18 lines were printed for Cellink® Bioink and Biogelx™-ink-RGD. The plates were analyzed by the cell confluence method in the multimode plate reader after 0, 2, 5, and 10min.

using the Anderson-Darling test, and one-way analysis of variance (ANOVA) was performed. An additional repeated-measures ANOVA was carried out during the examination of skrinkage behavior. Here, ANOVA was between the values for eacht point of time with time zero for each property of each plate. For all ANOVA investigations, α was set to 0.05 and a p-value below 0.05 was classified as statistically significant.

3. Results

3.1. Line analysis tool

In order to simplify the systematic process development in the field of 3D-bioprinting, the line analysis tool was established which enables a reproducible and automated analysis. At first, the applicability for bioinks with different optical properties was examined. It was started using Nivea® as a model ink with good optical properties, followed by experiments with Cellink Bioink due to its opaque appearance and due to the fact that it is a real bioink. Then, Biogelx™-ink-RGD was tested as it is more transparent and finally completely transparent Kolliphor solution was assessed. The results of Nivea® lines are shown in Fig. 3.

In each well of a six-well plate, a line was printed (n = 6) and was examined for length, width, and area. This was done for three plates so that in total, 18 lines were analyzed. Shown is the mean of length, width, and the area for each plate with standard deviation. The mean length is 29.1 mm (±0.2 mm), and the mean area is 38.9 mm^2 (±0.3 mm). Both properties are comparable for all three plates and not statistically significant. A statistical significance was found with a p-value of 0.007 for the width. The mean width of 0.64 mm by plate three differs from the mean value of 0.61 mm of plate one and plate two. Experiments using the more opaque Cellink ® Bioink and the more transparent Biogelx™-ink-RGD also showed a successful line detection and analysis. These two bioinks have been examined in more detail; the results are shown in Section 3.2. Kolliphor is a polymer which forms a completely transparent hydrogel after being dissolved and this hydrogel was also tested. Here, the object detection failed. In a subsequent approach, the contrast of Kolliphor solution was increased in three approaches with food coloring powder, paste, and Cochineal Red. The lines of these three approaches were also wrongly identified during image processing. The results are summarized in Table 2. A table showing exemplary pictures of typical detection and misdetection for the different materials can be found in the supplementary data.

3.2. Shrinkage study

Hydrogels have a high water content and over time, the water evaporates. The evaporation becomes visible by the shrinking of the bioprinted structures. The larger an object, the longer the printing time.

Table 2
Results of the line detection feasibility study with four bioinks.

Material	Correct line detection
Nivea®	√
Pure Kolliphor solution	×
Kolliphor with food coloring powder	×
Kolliphor with food coloring paste	×
Kolliphor with Cochineal Red	×
Cellink Bioink	√
Biogelx-ink-RGD	

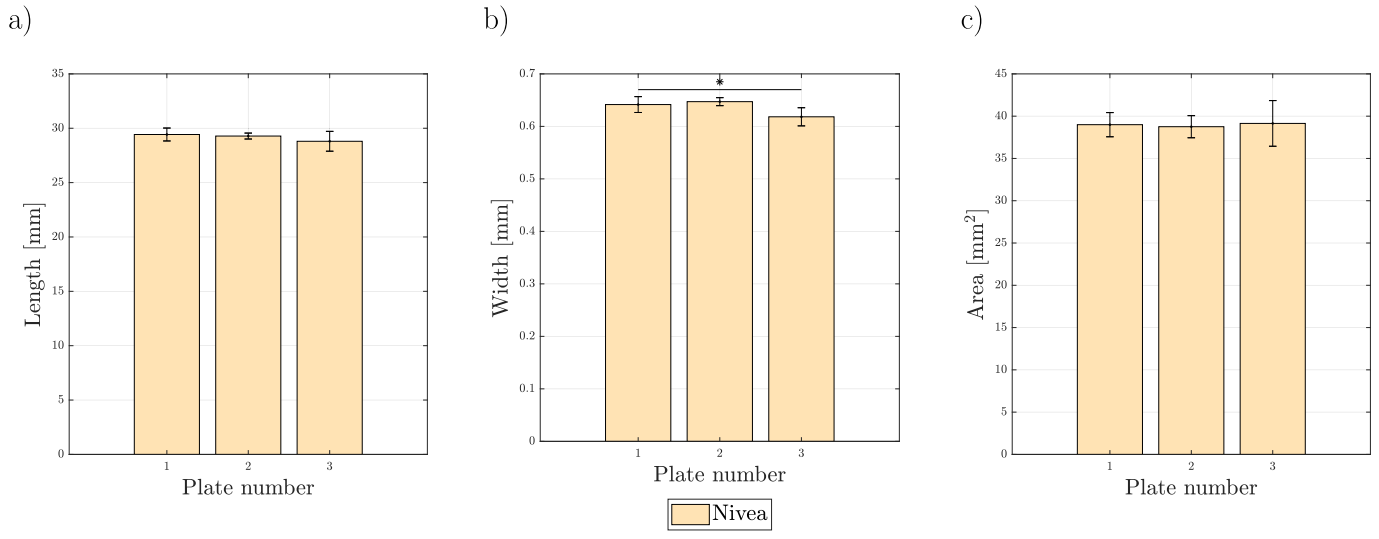

Fig. 3. Results of the analysis of 3 cm long printed lines with Nivea®. Length (a)), width (b)), and area (c)) were determined via image processing. Three plates were printed with six lines each (n = 6) resulting in 18 lines in total and compared as biological triplicates. Statistical significance (one-way ANOVA) was found for the width of the lines (p = 0.007).

Hence, it may start to shrink while it is still in production. A shrinkage study was conducted using the line analysis tool with Cellink® Bioink and Biogelx™-ink-RGD to assess whether the process time is a critical process parameter. The bioinks were chosen as both are already commercially available and are based on different materials. In addition, the results at time t = 0min were compared to investigate the reproducibility of the printing process. For each bioink, lines were printed in each well of a six-well plate (n = 6) and this was done as triplicate (n = 3) on three different days. In total, 18 lines per ink were printed and analyzed for t = 0, 2, 5, and 10min. For each point of time, the mean values for length, width, and area for each plate were calculated. The analysis of the lines directly after printing is shown in Fig. 4a)–c) and the results for Biogelx™-ink-RGD are displayed in d)-f). Based on the results, the reproducibility of the printing process was statistically examined.

The means of length, width, and area with standard deviation are plotted in a separate bar chart. The values were calculated based on the six lines of each plate at t = 0min and the results of the three plates are shown side by side for the respective properties. The results are visualized in a)-c) for Cellink® Bioink and in d)-f) for Biogelx™-ink-RGD. The mean length for Cellink ® Bioink is plotted in a). The maximum length is 28.56 mm and the minimum length is 28.56 mm. The mean width for Cellink® Bioink is from maximum 0.95 mm to minimum 0.83 mm. The maximum mean area is 53.44 mm^2 and the minimum is 46.21 mm^2. The values are comparable and during one-way ANOVA, no statistical significance was found.

For Biogelx™-ink-RGD, the averages of plates one and two were calculated based on five lines, because object detection failed for one line. In d), the length of Biogelx™-ink-RGD is in the range of minimum 28.29 mm to maximum 28.65 mm. The mean width is maximum 0.99 mm and minimum 0.9 mm. The maximum mean area is 6.57 mm^2 and the minimum mean area is 50.66 mm^2). Both, width and area, are higher in plate three than in plates one and two. For all three properties, the p-value was higher than 0.05 and no statistical significance (one-way ANOVA) was observed. To observe the shrinkage behavior of the bioinks, the same lines were again analyzed for all three properties using the identical method after two, five, and 10 min. The results are presented in Fig. 5 for Bioink and in Fig. 6 for Biogelx™-ink-RGD. For each plate length, width, and area are plotted as mean values of the six lines with associated standard deviation for the respective points in time. Here, each plate is shown in a separate row.

In general, the results shown in Fig. 5 reveal in all properties a declining trend which means that the size is shrinking with time. The

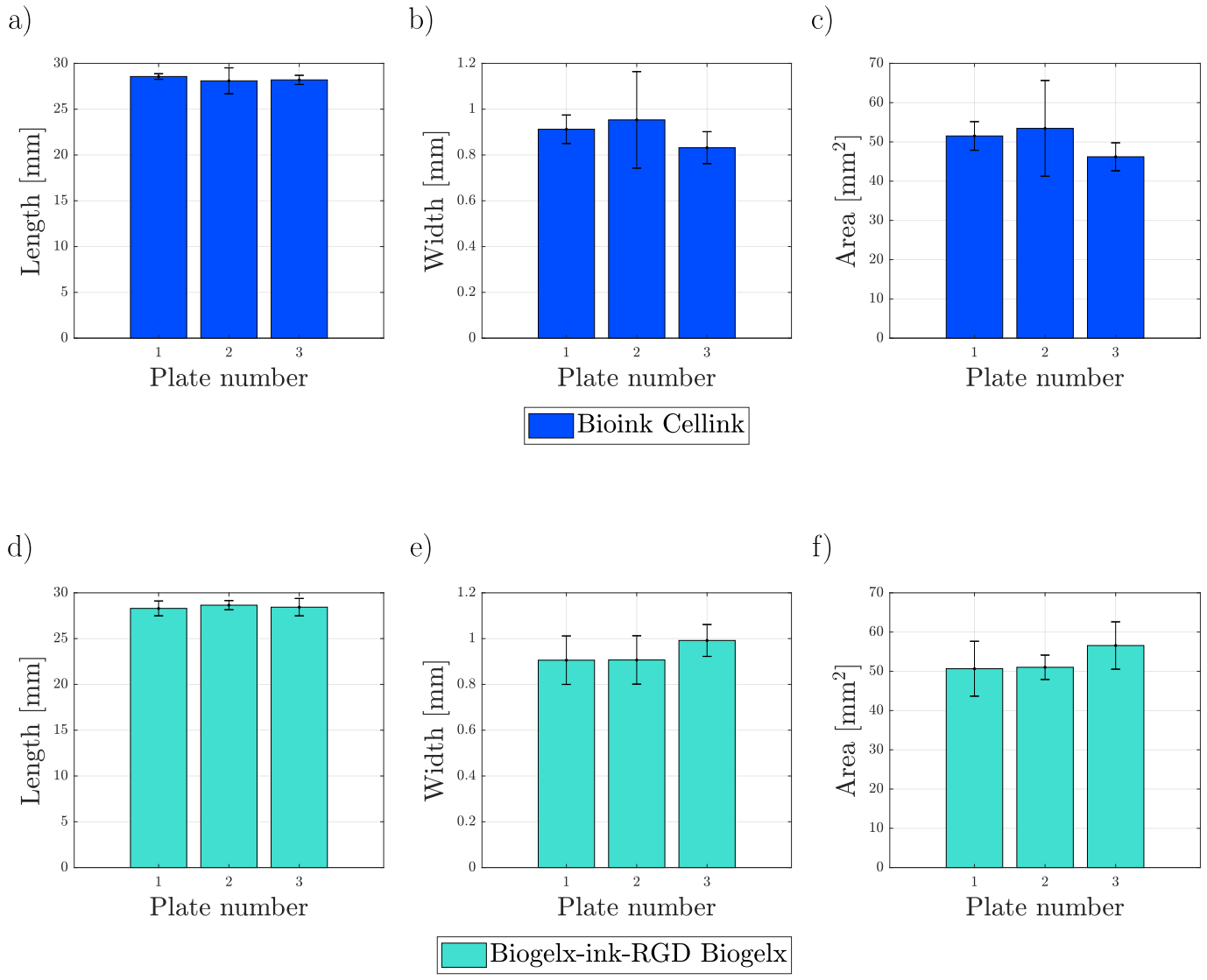

Fig. 4. Results of the analysis of 3 cm printed long lines in a)-c) with Cellink® Bioink and in d)-f) with Biogelx™-ink-RGD. Length, width, and area were determined via image processing directly after printing (t = 0min). The experiment was run as triplicate on three different days (n = 3) where one plate was printed. Six lines (n = 6) were printed on each plate, resulting in 18 lines in total, and no statistical significance (one-way ANOVA) was found for any property.

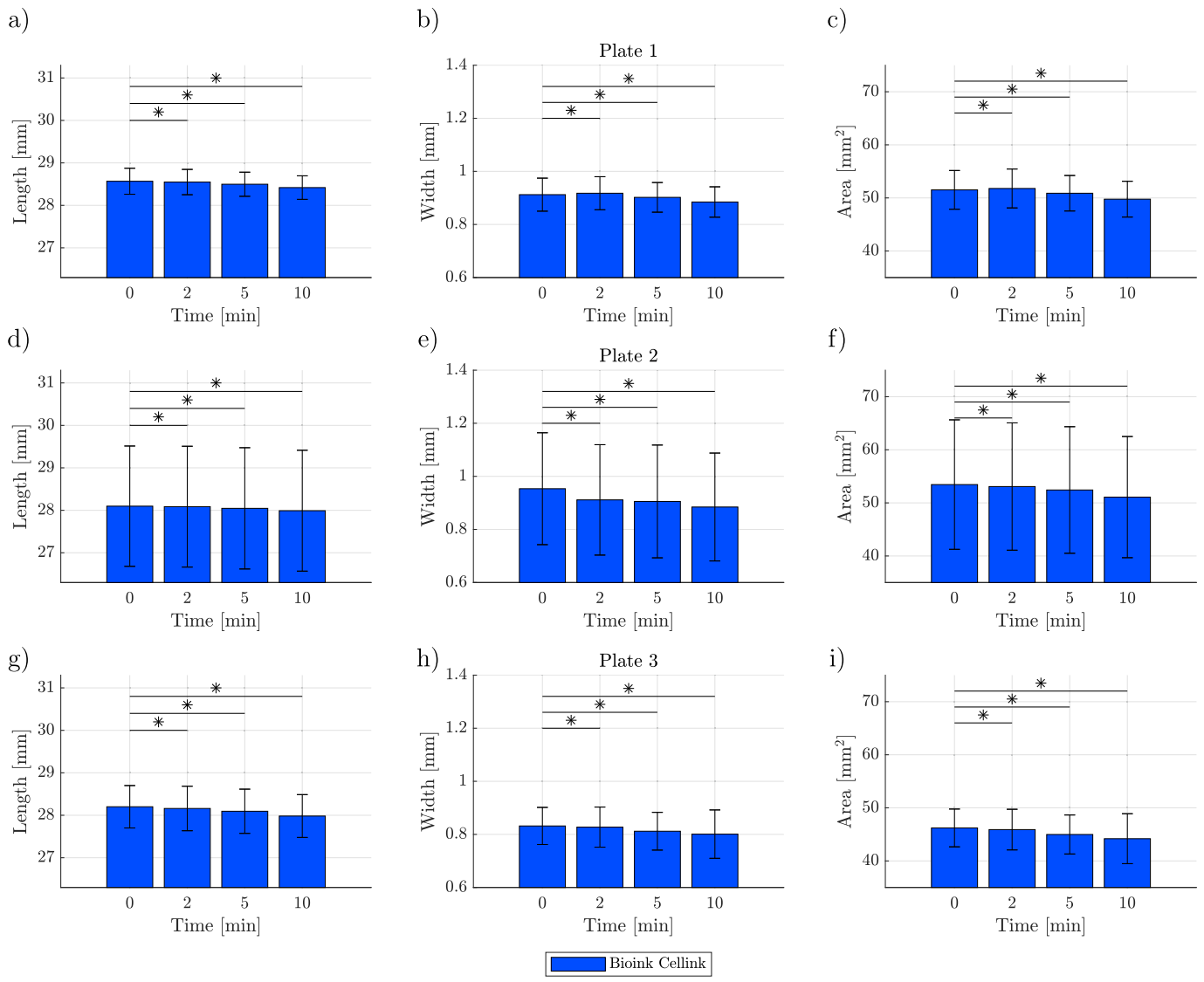

Fig. 5. Results of the analysis of 3 cm printed long lines with Cellink® Bioink. Six lines were printed per plate (n = 6) and the experiment was run as triplicate with three plates (n = 3) printed on three different days resulting in 18 lines in total. Length, width, and area were determined via image processing for different points in time (t = 0, 2, 5, and 10min). The results for plate one are shown in a)-c), for plate two in d)-f), and for plate three in g)-i). For length, width, and area, a repeated measures ANOVA analysis of all three plates showed statistical significance with p-values below 0.005.

standard deviation on plate two is a factor of three times higher in comparison to the other two plates. A repeated-measures ANOVA was performed for every property for all plates where mean values of the points of time were compared to time zero. For all data sets a statistical significance was found with p-values below 0.005. The statistical significance between the data sets is marked with an asterisk in the figure.

In Fig. 6, the length decreases constantly from 28.64 mm (±0.8 mm) to 28.44 mm (±0.3 mm) for plate two and from 28.43 mm (±0.9 mm) to 28.35 mm (±0.9 mm) for plate three. On the first plate, the length of 28.58 mm (±1 mm) measured after 5 min is higher than that of 27.96 mm (±1 mm) which was measured after 2 min. The same applies to the width. The width of plate two decreases from 0.9 mm (±0.05 mm) to 0.83 mm (±0.01 mm). The highest mean width was measured for plate three with a width of 0.99 mm (±0.07 mm) which drops to 0.94 mm (±0.08 mm). On plate one, the value of the width measured after 2 min is 0.86 mm (±0.12 mm) and increases to 0.98 mm (±0.14 mm) after 5 min. Also, the highest mean area was measured on plate three which decreased from 56.57 mm^2 (±6 mm^2) to 53.27 mm^2 (±5.68 mm^2) within 10 min. The mean area of plate two decreases from 51.02 mm^2 (±3.1 mm^2) to 48.47 mm^2 (±3.08 mm^2). On plate one, there is again an increase in the mean area after 2 min from 47.81 mm^2 (±8.36 mm^2) to 52.71 mm^2 (±10.91 mm^2). Except for the length of plate one with a p-value of 0.437, repeated-measures ANOVA analysis of all three plates showed a statistical significance between the data sets with p-values below 0.005. The statistical significance between the data sets is again marked with an asterisk in the figure.

4. Discussion

In order to simplify the process development for bioprinting, especially cell based applications where material thickness plays a major role, the image-based line analysis tool was developed to characterize the length, width, and area reproducibly. This tool is intended to make the printing process safer for clinical applications and facilitates the evaluation of printed lines. As automated imaging of 3d-printed objects is not yet possible with the in house tested commercially available cameras incorporated into 3d-printers, images were generated offline. For example one camera is oriented at a certain angle so that an imaging of objects within a well is not possible. Also, the camera's focus is fixed to the needle and it is not possible to take a photo automated after having

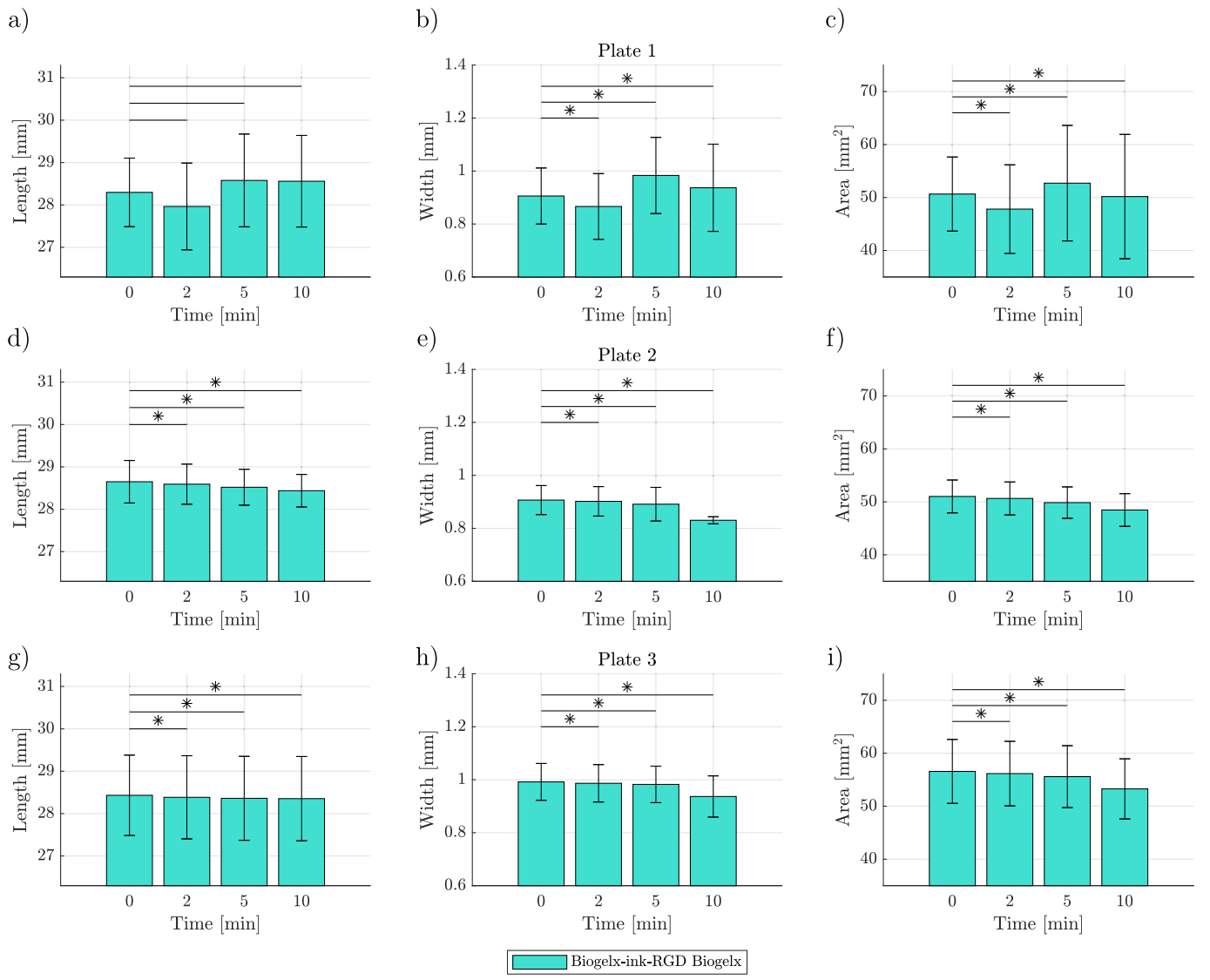

Fig. 6. Results of the analysis of 3 cm long printed lines with Biogelx™-ink-RGD (n = 6). Six lines were printed per plate (n = 6) and the experiment was run as triplicate with three plates (n = 3) printed on three different days resulting in 18 lines in total. Length, width, and area were determined via image processing for different points in time (t = 0, 2, 5, and 10min). The results for plate one are shown in a)-c), for plate two in d)-f), and for plate three in g)-i). Repeated-measures ANOVA analysis of all three plates showed statistical significance with p-values below 0.005. Only the length of the first plate shows no statistical significance with a p-value of 0.437.

finished the bioprint. Additionally the quality is not high enough for further image processing. Thus, imaging was done using a multiwell-plate reader as it easily enables an automated imaging for each well with the same method under an identical illumination set up. The developed method is important because it allows the analysis of a simple structure. Each complex geometry can be traced back to a few simple geometries and if already the first layer of an 3d-printed object is defective then this affects the entire 3D structure as the layers no longer adhere properly to one another. Of course, the line analysis is a first step but other structures such as circles and angle accuracy should be analyzed as well. Another possibility is to use the method for the comparison and characterization of bioprinting systems which again is important to increase reproducibility.

At first, the method was tested with model ink Nivea® as used as standard or control for pretests in 3d-printing processes [41]. Nivea® can be used for pretests without bioactive molecules as it is lacking biocompatibility but as Paxton [27] already argued it “is cheap, has a constant quality and composition, and is an example of a soft colloidal ink. Amongst other products, Nivea Crème, which has been established by bioprinter manufacturing company RegenHU (Switzerland) as demonstration ink, shows very good print fidelity."

On three days, one cartridge was prepared and one plate printed so that the experiment was run as a biological triplicate. An image was taken from each of the six lines of each plate and was imported into Matlab® and evaluated using the image processing method. During image processing, all Nivea® lines were detected correctly as objects. The line widths showed a statistical significance between the data sets for each plate, which means that they differ from each other, although all lines were printed under the same conditions using identical printing parameters. All line widths are bigger than the nozzle diameter of 0.26 mm due to expansion. The deviations are due to changes within the printer system. The printer system does not work reprodicibly and differences in applied pressure, speed, and offset can occur. Line width is a sensitive parameter in which slight variations are directly visible. Due to the different compositions of bioinks, they also have different optical properties. Therefore, the limitations of the method were investigated. In the following attempts to analyze lines printed with pure and colored Kolliphor solutions, object detection failed. The reason is the transparency of

material which is caused by the high water content of the hydrogel. Light is reflected on the object surface and creates bright areas. During the binarization step, these areas are transferred to white pixels so that the object contour is interrupted and the algorithm recognizes the object only partially. On the other hand, both bioinks, Bioink and Biogelx™-ink-RGD, are more opaque and can again be recognized by the algorithm. They have ingredients that lead to light scattering which prevents light reflections. As the bioinks have a high water content and the water evaporates over time, the line analysis tool was then applied to investigate whether the process time is a critical process parameter. A shrinkage study was conducted where all lines were analyzed directly after printing and again after 2, 5, and 10min. In addition, all lines were compared at time t = 0min to investigate whether they differ significantly statistically and to evaluate the reproducibility of the printing process. On two plates, one Biogelx™-ink-RGD line was detected incorrectly. Biogelx™-ink-RGD is more transparent than Cellink ® Bioink. Thus, again, high transparency leads to fail detection. By comparing the lines right after printing, there was no statistical significance found between the mean data sets of each plate. Especially the lengths of the lines are comparable, as a maximum mean length for Cellink® Bioink was measured to be 28.56 mm (±0.31 mm) and a minimum length to be 28.09 mm (±1.4 mm). The mean length of Biogelx™-ink-RGD was from maximum 28.65 mm (±0.5 mm) to minimum 28.3 mm (±0.81 mm). The width measured with Cellink® Bioink ranges from maximum 0.95 mm (±0.96 mm) to a minimum width of 0.83 mm (±0.99 mm). With Biogelx™-ink-RGD the width varies from maximum 0.99 mm (±0.06 mm) to minimum 0.91 mm (±0.11 mm). Also, the area varies in a range from maximum 56.67 mm^2 (±6.99 mm) for plate three with Biogelx™-ink-RGD to a minimum area of 46.22 mm^2 (±3.55 mm^2) on plate three for Cellink® Bioink. The widths and areas are more sensitive to fluctuations within the printer system. When considering the high water content of hydrogels and the change in properties over time, the shrinkage of the lines becomes obvious. The water evaporates and hence the size of the lines changing decreases. For building up a 3D model, the printing time and the change of the object height should be considered and can be limiting [42]. If an object is built with many layers, the height is calculated for each layer. The larger the object, the longer the printing process. If this takes too long, the object will start to shrink and the layer height will not be correct after a certain time. This will cause the object to become faulty. As a result, the process time is a critical process parameter which poses two problems. Firstly, the printing time or the CAD model must be optimized or shrinkage can be prevented by a regulated humidity chamber. Secondly, the analysis of printed objects must be carried out immediately after printing and as quickly as possible because the properties already change after a few minutes. A general disadvantage of the used method is the long imaging process when using the plate reader because it takes 2min to generate one picture for one well. It can be assumed that the high water content of bioinks decreases especially at the beginning. On the other hand, the constant conditions are advantageous, as the illumination and recording settings are always the same. For future applications, a set-up has to be found which enables a fast imaging process with a proper illumination which allows the analysis of transparent bioinks. The shrinkage behavior should be evaluated again with a more suitable set-up. The change in size is also confirmed by the significance in the repeated-measures ANOVA. Here, the data sets of all points in time were examined for statistical significance with time zero. The data at different points in time are differing and are not comparable. One exception is plate one of Biogelx™-ink-RGD. Here, the lines seem to grow in time, but this can be a detection problem due to the bioink's transparency.

5. Conclusion

Imaging-based analysis methods are promising PAT-tools for evaluating 3D-printed objects. These can be applied for printer characterization, for evaluating the printability of bioinks, and for optimization of printing processes in a non-invasive way in order to facilitate the application of bioprinting in the fields of regenerative medicine (RM) and tissue engineering (TE) [1,2]. The established method was applied successfully for printed-line characterization. A first layer characterization is important as the printing accuracy for simple structures can be analyzed and a correct first layer is important to build up a whole object in layers. Object heights can also be analyzed by image processing. The length, area, and width can be determined. A new criterion and strategy were introduced to calculate the width within a stable area, otherwise a wide variation for width determination is possible. Nevertheless, the method showed some limitation during pre-tests. At current state, light reflections cause a discontinuous object contour for transparent materials and therefore the objects are detected incorrectly. For future application, the lighting has to be optimized to achieve an appropriate illumination. The second limitation is the speed of the imaging process as the image generation takes 2min in the cell confluence method. Nevertheless, a shrinkage behavior of bioinks has been demonstrated and should be considered for planing bioprinting processes. In general, the image processing method can be adapted to arbitrary image files and is a progress because multiple images can be analyzed in a completely automated way. This is a progress for systematic process development and a prerequisite for the transfer from research to clinical applications and industry. Advantageous is the high reproducibility and the minimization of variation as it is independent of the user. At the same time, it is a robust and time-saving method as the user can analyze all images at once.

CRediT authorship contribution statement

Svenja Strauß: Conceptualization, Methodology, Software, Writing - original draft. **Rafaela Meutelet:** Investigation. **Luka Radosevic:** Experimental work. **Sarah Gretzinger:** Conceptualization, Writing - review & editing. **Jürgen Hubbuch:** Conceptualization, Writing - review & editing.

Declaration of competing interest

The authors declare that they have no known competing financial interests or personal relationships that could have appeared to influence the work reported in this paper.

Acknowledgments

This work was funded by the German Federal Ministry of Education and Research (BMBF) as project SOP-Bioprint under contract number 13XP5071B.

Appendix A. Supplementary data

Supplementary data to this article can be found online at https://doi.org/10.1016/j.bprint.2020.e00112.

References

[1] J. Groll, T. Boland, T. Blunk, J.A. Burdick, D.-W. Cho, P.D. Dalton, B. Derby, G. Forgacs, Q. Li, V.A. Mironov, L. Moroni, M. Nakamura, W. Shu, S. Takeuchi, G. Vozzi, T.B.F. Woodfield, T. Xu, J.J. Yoo, J. Malda, Biofabrication: reappraising the definition of an evolving field, Biofabrication 8 (1) (2016), 013001, https://doi.org/10.1088/1758-5090/8/1/013001.

[2] S. Duin, K. Schütz, T. Ahlfeld, S. Lehmann, A. Lode, B. Ludwig, M. Gelinsky, 3d bioprinting of functional islets of langerhans in an alginate/methylcellulose hydrogel blend, Advanced Healthcare Materials 8 (7) (2019), 1801631, https://doi.org/10.1002/adhm.201801631.

[3] J. Malda, J. Visser, F.P. Melchels, T. Jüngst, W.E. Hennink, W.J.A. Dhert, J. Groll, D.W. Hutmacher, 25th anniversary article: engineering hydrogels for biofabrication, Adv. Mater. 25 (36) (2013) 5011–5028, https://doi.org/10.1002/adma.201302042.

[4] A. Atala, Engineering organs, Curr. Opin. Biotechnol. 20 (5) (2009) 575–592, https://doi.org/10.1016/j.copbio.2009.10.003.

[5] S. Murphy, A. Atala, 3d bioprinting of tissues and organs, Nat. Biotechnol. 32. doi: 10.1038/nbt.2958.

[6] F. Groeber, M. Holeiter, M. Hampel, S. Hinderer, K. Schenke-Layland, Skin tissue engineering — in vivo and in vitro applications, Adv. Drug Deliv. Rev. 63 (4) (2011) 352–366, https://doi.org/10.1016/j.addr.2011.01.005.

[7] T. Jungst, W. Smolan, K. Schacht, T. Scheibel, J. Groll, Strategies and molecular design criteria for 3d printable hydrogels, Chem. Rev. 116 (3) (2016) 1496–1539, https://doi.org/10.1021/acs.chemrev.5b00303.

[8] A.S. Hoffman, Hydrogels for biomedical applications, Adv. Drug Deliv. Rev. 64 (2012) 18–23, https://doi.org/10.1016/j.addr.2012.09.010.

[9] S. Krishnamoorthi, A. Banerjee, A. Roychoudhury, Immobilized enzyme technology: potentiality and prospects, J. Enzymol. Metabol. 1 (1) (2015), 010–104.

[10] B. Schmieg, A. Schimek, M. Franzreb, Development and performance of a 3d-printable poly(ethylene glycol) diacrylate hydrogel suitable for enzyme entrapment and long-term biocatalytic applications, Eng. Life Sci. 18 (9) (2018) 659–667, https://doi.org/10.1002/elsc.201800030.

[11] B. Schmieg, M. Nguyen, M. Franzreb, Simulative minimization of mass transfer limitations within hydrogel-based 3d-printed enzyme carriers, Frontiers in Bioengineering and Biotechnology 8 (2020) 365, https://doi.org/10.3389/fbioe.2020.00365.

[12] K.Y. Leee, D.J. Mooney, Hydrogels for tissue engineering, Chem. Rev. 101 (7) (2001) 1869–1879, https://doi.org/10.1021/cr000108x.

[13] J. Zhu, Bioactive modification of poly(ethylene glycol) hydrogels for tissue engineering, Biomaterials 31 (17) (2010) 4639–4656, https://doi.org/10.1016/j.biomaterials.2010.02.044.

[14] T. Vermonden, R. Censi, W.E. Hennink, Hydrogels for protein delivery, Chem. Rev. 112 (2012) 2853–2888, https://doi.org/10.1021/cr200157d.

[15] A.G. Tabriz, M.A. Hermida, N.R. Leslie, W. Shu, Three-dimensional bioprinting of complex cell laden alginate hydrogel structures, Biofabrication 7 (4) (2015), 045012, https://doi.org/10.1088/1758-5090/7/4/045012.

[16] T.T. Demirtaş, G. Irmak, M. Gümüşderelioğlu, A bioprintable form of chitosan hydrogel for bone tissue engineering, Biofabrication 9 (3) (2017), 035003, https://doi.org/10.1088/1758-5090/aa7b1d.

[17] J.Y. Park, J.-C. Choi, J.-H. Shim, J.-S. Lee, H. Park, S.W. Kim, J. Doh, D.-W. Cho, A comparative study on collagen type i and hyaluronic acid dependent cell behavior for osteochondral tissue bioprinting, Biofabrication 6 (3) (2014), 035004, https://doi.org/10.1088/1758-5082/6/3/035004.

[18] J.D. Kosmala, D.B. Henthorn, L. Brannon-Peppas, Preparation of interpenetrating networks of gelatin and dextran as degradable biomaterials, Biomaterials 21 (20) (2000) 2019–2023, https://doi.org/10.1016/S0142-9612(00)00057-0.

[19] B.V. Slaughter, S.S. Khurshid, O.Z. Fisher, A. Khademhosseini, N.A. Peppas, Hydrogels in regenerative medicine, Adv. Mater. 21 (32–33) (2009) 3307–3329, https://doi.org/10.1002/adma.200802106.

[20] M. Du, B. Chen, Q. Meng, S. Liu, X. Zheng, C. Zhang, H. Wang, H. Li, N. Wang, J. Dai, 3d bioprinting of BMSC-laden methacrylamide gelatin scaffolds with CBD-BMP2-collagen microfibers, Biofabrication 7 (4) (2015), 044104, https://doi.org/10.1088/1758-5090/7/4/044104.

[21] S. Naahidi, M. Jafari, M. Logan, Y. Wang, Y. Yuan, H. Bae, B. Dixon, P. Chen, Biocompatibility of hydrogel-based scaffolds for tissue engineering applications, Biotechnol. Adv. 35 (5) (2017) 530–544, https://doi.org/10.1016/j.biotechadv.2017.05.006.

[22] R.A. Scott, N.A. Peppas, Highly crosslinked, peg-containing copolymers for sustained solute delivery, Biomaterials 20 (15) (1999) 1371–1380, https://doi.org/10.1016/S0142-9612(99)00040-X.

[23] S. Bertlein, G. Brown, K.S. Lim, T. Jungst, T. Boeck, T. Blunk, J. Tessmar, G.J. Hooper, T.B.F. Woodfield, J. Groll, Thiol–ene clickable gelatin: a platform bioink for multiple 3d biofabrication technologies, Adv. Mater. 29 (44) (2017), 1703404, https://doi.org/10.1002/adma.201703404.

[24] A.C. Jen, M.C. Wake, A.G. Mikos, Review: hydrogels for cell immobilization, Biotechnol. Bioeng. 50 (4) (1996) 357–364, https://doi.org/10.1002/(SICI)1097-0290(19960520)50:4<357::AID-BIT2>3.0.CO;2-K.

[25] K. Yue, G.T. de Santiago], M.M. Alvarez, A. Tamayol, N. Annabi, A. Khademhosseini, Synthesis, properties, and biomedical applications of gelatin methacryloyl (gelma) hydrogels, Biomaterials 73 (2015) 254–271, https://doi.org/10.1016/j.biomaterials.2015.08.045.

[26] L. Wenger, C. Radtke, J. Göpper, M. Wörner, J. Hubbuch, 3d-printable and enzymatically active composite materials based on hydrogel-filled high internal phase emulsions, Frontiers in Bioengineering and Biotechnology 8 (2020) 713, https://doi.org/10.3389/fbioe.2020.00713.

[27] N. Paxton, W. Smolan, T. Böck, F. Melchels, J. Groll, T. Jungst, Proposal to assess printability of bioinks for extrusion-based bioprinting and evaluation of rheological properties governing bioprintability, Biofabrication 9 (4) (2017), 044107, https://doi.org/10.1088/1758-5090/aa8dd8.

[28] T. Gao, G.J. Gillispie, J.S. Copus, A.K. Pr, Y.-J. Seol, A. Atala, J.J. Yoo, S.J. Lee, Optimization of gelatin–alginate composite bioink printability using rheological parameters: a systematic approach, Biofabrication 10 (3) (2018), 034106, https://doi.org/10.1088/1758-5090/aacdc7.

[29] K. Markstedt, A. Mantas, I. Tournier, H. Martínez Ávila, D. Hägg, P. Gatenholm, 3D bioprinting human chondrocytes with nanocellulose-alginate bioink for cartilage tissue engineering applications, Biomacromolecules 16 (5) (2015) 1489–1496, https://doi.org/10.1021/acs.biomac.5b00188.

[30] T. Lorson, S. Jaksch, M.M. Lübtow, T. Jüngst, J. Groll, T. Lühmann, R. Luxenhofer, A thermogelling supramolecular hydrogel with sponge-like morphology as a cytocompatible bioink, Biomacromolecules 18 (7) (2017) 2161–2171, https://doi.org/10.1021/acs.biomac.7b00481.

[31] N. Soltan, L. Ning, F. Mohabatpour, P. Papagerakis, X. Chen, Printability and cell viability in bioprinting alginate dialdehyde-gelatin scaffolds, ACS Biomater. Sci. Eng. 5 (6) (2019) 2976–2987, https://doi.org/10.1021/acsbiomaterials.9b00167.

[32] B. Webb, B.J. Doyle, Parameter optimization for 3d bioprinting of hydrogels, Bioprinting 8 (2017) 8–12, https://doi.org/10.1016/j.bprint.2017.09.001.

[33] A. Ribeiro, M.M. Blokzijl, R. Levato, C.W. Visser, M. Castilho, W.E. Hennink, T. Vermonden, J. Malda, Assessing bioink shape fidelity to aid material development in 3d bioprinting, Biofabrication 10 (1) (2017), 014102, https://doi.org/10.1088/1758-5090/aa90e2.

[34] E.N. Malamas, E.G. Petrakis, M. Zervakis, L. Petit, J.-D. Legat, A survey on industrial vision systems, applications and tools, Image Vis Comput. 21 (2) (2003) 171–188, https://doi.org/10.1016/S0262-8856(02)00152-X.

[35] L.S. Chow, R. Paramesran, Review of medical image quality assessment, Biomed. Signal Process Contr. 27 (2016) 145–154, https://doi.org/10.1016/j.bspc.2016.02.006.

[36] F. M. Wunner, P. Mieszczanek, O. Bas, S. Eggert, J. Maartens, P. D. Dalton, E. M. De-Juan-Pardo, D. W. Hutmacher, Printomics: the high-throughput analysis of printing parameters applied to melt electrowriting, Biofabrication 11. doi:10.1088/1758-5090/aafc41.

[37] F. Yang, H. Zhao, Q. Gao, B. Xia, F. Jianzhong, Research on the printability of hydrogels in 3d bioprinting, Sci. Rep. 6 (2016) 29977, https://doi.org/10.1038/srep29977.

[38] Q. Gao, X. Niu, L. Shao, L. Zhou, Z. Lin, A. Sun, J. Fu, Z. Chen, J. Hu, Y. Liu, Y. He, 3d printing of complex GelMA-based scaffolds with nanoclay, Biofabrication 11 (3) (2019), 035006, https://doi.org/10.1088/1758-5090/ab0cf6.

[39] M. Alonzo, E. Dominguez, F. Alvarez-Primo, A. Quinonez, E. Munoz, J. Puebla, A. Barron, L. Aguirre, A. Vargas, J.M. Ramirez, B. Joddar, A comparative study in the printability of a bioink and 3d models across two bioprinting platforms, Mater. Lett. 264 (2020), 127382, https://doi.org/10.1016/j.matlet.2020.127382.

[40] M. K. Włodarczyk-Biegun, J. I. Paez, M. Villiou, J. Feng, A. del Campo, Printability Study of Metal Ion Crosslinked Peg-Catechol Based Inks, bioRxiv doi:10.1101/599290.

[41] C.P. Radtke, N. Hillebrandt, J. Hubbuch, The biomaker: an entry-level bioprinting device for biotechnological applications, J. Chem. Technol. Biotechnol. 93 (3) (2018) 792–799, https://doi.org/10.1002/jctb.5429.

[42] T. Billiet, M. Vandenhaute, J. Schelfhout, S.V. Vlierberghe], P. Dubruel, A review of trends and limitations in hydrogel-rapid prototyping for tissue engineering, Biomaterials 33 (26) (2012) 6020–6041, https://doi.org/10.1016/j.biomaterials.2012.04.050.